ELSEVIER

Journal of Magnetism and Magnetic Materials 239 (2002) 255–260

Journal of magnetism and magnetic materials

www.elsevier.com/locate/jmmm

Magneto-optical Kerr effects in metallic superlattices fabricated by monatomic layer control—comparison between experiments and first-principles calculations

Masatake Yamaguchi[a], Koki Takanashi[b,*], Kiyokazu Himi[b], Koji Hayata[c], Katsuaki Sato[c], Hiroyasu Fujimori[d]

[a] *Center for Promotion of Computational Science and Engineering, Japan Atomic Energy Research Institute, Tokai-mura, Ibaraki 319-1195, Japan*

[b] *Institute for Materials Research, Tohoku University, 2-1-1 Katahira, Aoba-ku, Sendai, Miyagi 980-8577, Japan*

[c] *Faculty of Technology, Tokyo University of Agriculture and Technology, Koganei, Tokyo 184-8588, Japan*

[d] *Research Institute for Electronic and Magnetic Materials, Yagiyama-minami 2-1-1, Tihaku-ku, Sendai, Miyagi 982-0807, Japan*

Abstract

The magneto-optical Kerr effects in metallic superlattices (Fe/Au, Co/Ru) fabricated by monatomic layer control technique were measured and compared with first-principles calculations. For Fe/Au, the measured Kerr spectra of Fe(x ML)/Au(x ML) ($x = 1-6$, ML: monatomic layer thickness) showed systematic change with the change of layer thickness x. For Co/Ru, the measured Kerr rotation angle of Co(5 ML)/Ru(5 ML) was almost ten times smaller than that of HCP Co. The calculated results from first-principles were in reasonable agreement with the experimental results. The characteristics of the spectra can be understood from the analysis of the electronic structure.

Keywords: Magneto-optical Kerr effect; First-principles calculations; Metallic superlattice

1. Introduction

Recently, the development of thin film preparation techniques has realized monatomic layer control of metal elements. In previous papers [1,2], we reported on the artificial fabrication of an $L1_0$ ordered FeAu alloy by the alternate deposition of Fe(0 0 1) and Au(0 0 1) monatomic layers although Fe and Au are immiscible and no intermediate phase exists in the equilibrium phase diagram. The $L1_0$ ordered FeAu alloy is ferromagnetic, and it possesses a large Fe moment exceeding 2.2 μ_B and a large uniaxial anisotropy with the easy axis along [0 0 1]; therefore, the film is perpendicularly magnetized. Fe(x ML)/Au(x ML) superlattices ($x > 1$, ML: monatomic layer thickness) were also prepared, and these magnetic properties were compared to those for $x = 1$, i.e., the $L1_0$ ordered FeAu alloy. The perpendicular magnetic anisotropy was found to oscillate as a function of x with a period of 1 ML, reflecting the change in interface morphology [3]; this confirms the precise layer thickness control on a monatomic layer scale for our samples.

The Fe(x ML)/Au(x ML) superlattices were simply ferromagnetic with uniform magnetic structure for $x < 5$. For the artificial modulation of magnetic structure, Co and Ru have been selected as constituents of superlattices in the next step. Several studies were made to date for Co/Ru superlattices with comparatively large Co thicknesses [4–6], which showed strong antiferromagnetic coupling of Co even for a few atomic layers of the Ru thickness. This suggests the possibility that alternating Co and Ru on a monatomic layer scale might

*Corresponding author: Tel.: +81-22-215-2095; fax: +81-22-215-2096.

E-mail address: koki@imr.tohoku.ac.jp (K. Takanashi).

0304-8853/02/$ - see front matter
PII: S0304-8853(01)00566-2

form an artificial antiferromagnet. In the equilibrium phase diagram, Co and Ru form solid solutions for all the compositions, and no ordered structure exists. However, the good epitaxial growth for HCP Co/Ru(0001) can be realized in spite of a considerably large lattice mismatch (~7.4%) [7]. We have actually succeeded in the artificial fabrication of an ordered CoRu alloy with alternate stacking of HCP Co(0001) and Ru (0001) monatomic layers [8] and Co/Ru superlattices with a variety of Co and Ru thicknesses up to 5 ML. Only 1 ML difference in the Co or Ru thickness has a strong influence on the indirect exchange coupling of Co through Ru. First-principles calculations supported the fact that the difference in Ru thickness critically affected the indirect exchange coupling [8,9].

The fabrication of magnetic superlattices by monatomic layer control makes it possible to compare their properties directly with the calculated results from first-principles. The indirect exchange coupling of Fe through Au was investigated using Brillouin light scattering [10]. The coupling was always ferromagnetic for $x<5$, and the strength showed oscillatory behavior as a function of x. The first-principles calculations were in excellent agreement with the experiments [10,11].

The magneto-optical Kerr spectra were also measured and compared with the first-principles calculations. For Fe/Au, the measured Kerr spectra changes systematically for Fe(x ML)/Au(x ML) ($x=1-15$). First-principles calculations reproduced the shape of Kerr spectra and the trend of this change with x. In addition, we found the characteristic optical transition which determines the shape of Kerr spectra [12–14].

In this paper, we show the results of the measured and calculated Kerr spectra of a Co(5 ML)/Ru(5 ML) superlattice with a brief review about Kerr spectra of Fe/Au superlattices. The measured Kerr rotation angle of Co(5 ML)/Ru(5 ML) is almost ten times smaller than that of HCP Co in the range of 1–5 eV. We have calculated the Kerr spectrum from first-principles and found that the small Kerr rotation angle can be well understood from the band theory.

2. Procedures

2.1. Sample preparation and measurement of Kerr spectra

Samples were prepared through the use of an ultrahigh vacuum (UHV) electron beam evaporation method with monatomic layer control. Fe/Au(001) superlattices were grown on Au(001) buffers deposited on MgO(001) substrates. Co/Ru(0001) superlattices were grown on Ru(0001) buffers deposited on sapphire($11\bar{2}0$) substrates. Epitaxial growth was confirmed by RHEED patterns. X-ray diffraction measurements and transimission electron microscopy observations indicated the existence of superstructure. The details on sample preparation and structural characterization were described in previous papers [1,2,8].

Spectra of the magneto-optical Kerr effects were measured at room temperature employing a Kerr spectrometer [15] with a polarization modulation technique using a photoelastic modulator. The measurements provided both Kerr rotation and ellipticity spectra. The samples were saturated with a perpendicular magnetic field with a flux density of 1.7 T.

2.2. The method of calculations

The ground state (scalar-relativistic) electronic structures were calculated by the LMTO-ASA method based on local-spin density approximation (LSDA). Then, the spin–orbit interaction was included in a perturbative way. Using the calculated energy eigenvalues and wave functions, the real part of the diagonal conductivity $\mathrm{Re}(\sigma_{xx})$ and imaginary part of the off-diagonal one $\mathrm{Im}(\sigma_{xy})$ due to interband transition were calculated from the equations derived by Wang and Callaway [16]. Then, $\mathrm{Im}(\sigma_{xx})$ and $\mathrm{Re}(\sigma_{xy})$ were calculated from the Kramers–Kronig transformation of the $\mathrm{Re}(\sigma_{xx})$ and $\mathrm{Im}(\sigma_{xy})$, respectively. To introduce the effect of life time, σ_{xx} and σ_{xy} were smoothed by the Lorentz relaxation, in which the parameter of the relaxation was chosen as 0.5 eV. Then, the polar Kerr rotation angle $\theta_K(\omega)$ and ellipticity $\varepsilon_K(\omega)$ [rad] were calculated by

$$\begin{aligned}\theta_K + i\varepsilon_K &= -\frac{\sigma_{xy}}{\sigma_{xx}\sqrt{1+i(4\pi/\omega)\sigma_{xx}}} = \frac{\omega\sigma_{xy}}{D} \\ &= \mathrm{Re}(\omega\sigma_{xy})\,\mathrm{Re}(1/D) - \mathrm{Im}(\omega\sigma_{xy})\mathrm{Im}(1/D) \\ &\quad + i\{\mathrm{Re}(\omega\sigma_{xy})\,\mathrm{Im}(1/D) + \mathrm{Im}(\omega\sigma_{xy})\,\mathrm{Re}(1/D)\},\end{aligned} \tag{1}$$

where D is defined for the discussion in the next section. Using the calculated energy of plasma frequency ($\hbar\omega_p$), Drude term was calculated and added to σ_{xx}. More details about our calculations are summarized in previous papers [13,14].

3. Results and discussion

3.1. Fe/Au superlattices

In Fig. 1, the experimental and calculated Kerr spectra for Fe(x ML)/Au(x ML) ($x=1-6$) are shown [12–14]. In the case of $x=1$, the crystal structure is an ordered $L1_0$-type structure. The dashed line indicates another calculated result using different atomic sphere radii. In the range of 6–7 eV we can see a large difference, which is due to the well-known fact that the

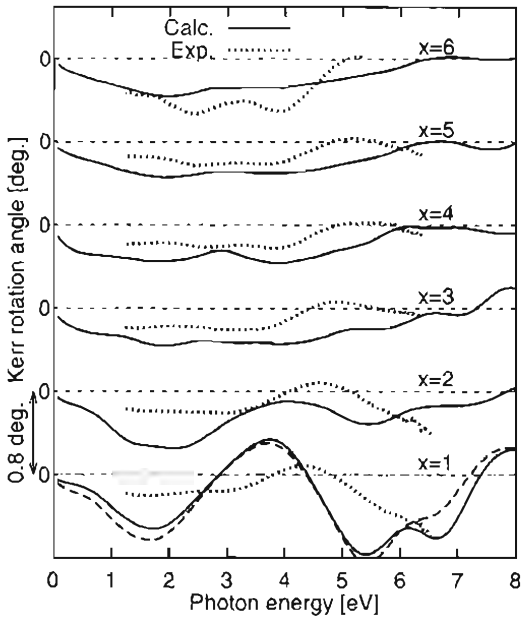

Fig. 1. Calculated (solid line) and experimental (dotted line) Kerr spectra of Fe(x ML)/Au(x ML) superlattices ($x = 1-6$). The dashed line indicates the result calculated using a different ratio between the radii of Fe and Au atomic spheres.

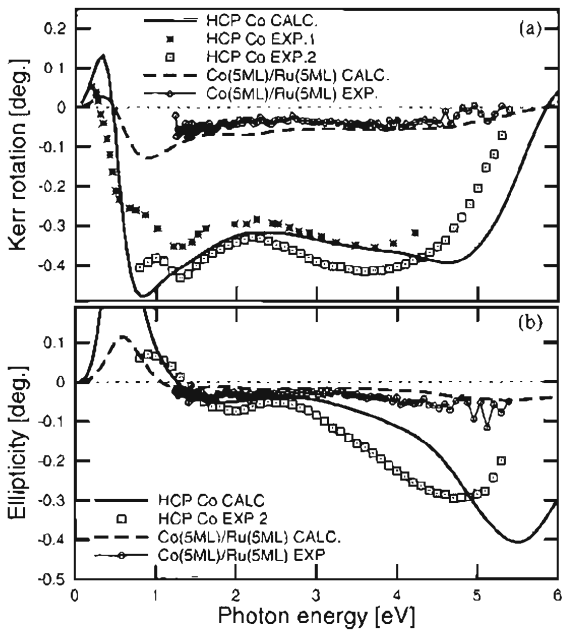

Fig. 2. (a) Kerr rotation and (b) ellipticity spectra of Co(5 ML)/Ru(5 ML). The calculated $\hbar\omega_p$ is 5 eV. For comparison, those of HCP Co are also shown. Experimental data of HCP Co are in Ref. [17].

energy eigenvalues of unoccupied states in high energy depend on the choice of atomic sphere radii in the LMTO-ASA calculations.

In our calculated results, the peak structure at about 4 eV shifts towards higher energies and the large Kerr rotation angle around 6 eV decreases with an increase of x. These trends are in good agreement with experimental data. From the detailed analysis of the band structure and transition matrix elements, it was found that the peak structure around 4 eV in the case of $x = 1$ originates mainly from the $d_\downarrow \rightarrow f_\downarrow$ transition at the atomic site of Au, in which the final state $5f_\downarrow$ is the one hybridized with the adjacent Fe($3d_\downarrow$) states. In other words, this transition can be regarded as the Au($5d_\downarrow$) $\rightarrow$ Fe($3d_\downarrow$) transition, which was proposed by one of the authors (K.S.) from a simple analysis using density of states function. This peak shifts towards higher energies with an increase of x as stated above, which is due to the shift of final states towards higher energies.

3.2. Co/Ru superlattices

The magneto-optical Kerr effect has been found to decrease drasticlly by multilayering Co with Ru, compared with that for pure HCP Co. For an example, the measured and calculated spectra of Kerr rotation angle and ellipticity for a Co(5 ML)/Ru(5 ML) superlattice are shown in Figs. 2(a) and (b). The calculated spectra are in reasonable agreement with the measured spectra. For comparison, the spectra of HCP Co are also shown. Our calculated spectra of HCP Co are almost the same as the previous calculations by others [17].

The electronic structure of Co(5 ML)/Ru(5 ML) was calculated by LMTO-ASA method assuming indirect ferromagnetic coupling between Co layers through Ru layers. The in-plane lattice constant a is chosen as 2.706 Å, which is the same as HCP Ru. The out-of-plane lattice spacings are determined to be consistent with the X-ray diffraction profiles. The magnetic moment of Co layers are 1.45, 1.66, and 1.65 μ_B/Co in Co-layer that is adjacent to a Ru-layer, the next Co-layer, and central Co-layer, respectively. The experimental average magnetic moment is about 1.5 μ_B, which is very close to the calculated result.

As shown in Fig. 2(a), the Kerr rotation angle of Co(5ML)/Ru(5 ML) are almost ten times smaller than that of HCP Co. This was contrary to our first expectation that the Kerr rotation angle of Co(5 ML)/Ru(5 ML) should be at least half of HCP Co or more. For the first reason of this expectation, the indirect exchange coupling of this superlattice is ferromagnetic and the measured average magnetic moment of Co layers was 1.5 μ_B/Co, which is very close to that of HCP Co (1.7 μ_B/Co). For the second reason, 4d metal Ru has larger spin–orbit interaction than 3d metal Co. In this way, it seemed strange to us that only small Kerr rotation angle could be found for Co(5 ML)/Ru(5 ML). In the following, however, we can show some reasons

for the small Kerr rotation angle of this superlattice from first-principles calculations.

Kerr rotation angle is determined by not only off-diagonal conductivity (σ_{xy}) but also diagonal conductivity (σ_{xx}) as shown in Eq. (1). To observe σ_{xx} and its contribution to Kerr rotation angle, we show the calculated results of σ_{xx} and $1/D$ in Eq. (1) for Co(5 ML)/Ru(5 ML) in Fig. 3. For comparison, the calculated results for HCP Co, distorted HCP Co (denoted by d-Hcp Co), and HCP Ru are also shown. Here, the distorted HCP Co has the same in-plane lattice constant a as Co(5 ML)/Ru(5 ML) and has the same out-of-plane lattice spacing $c/2$ as the inside Co-layers in Co(5 ML)/Ru(5 ML).

From Figs. 3(a) and (b), we can see that both $\mathrm{Re}(\sigma_{xx})$ and $\mathrm{Im}(\sigma_{xx})$ of Co(5 ML)/Ru(5 ML) are made from a simple average between HCP Ru and distorted HCP Co except for low energy region (<1.5 eV). As a result, $\mathrm{Re}(\sigma_{xx})$ of Co(5 ML)/Ru(5 ML) is much larger than that of HCP Co since $\mathrm{Re}(\sigma_{xx})$ of HCP Ru is very large. This change in σ_{xx} causes the change in $1/D$ through Eq. (1) as seen in Figs. 3(c) and (d). Although $\mathrm{Re}(1/D)$ of Co(5 ML)/Ru(5 ML) is almost the same as that of HCP Co, $\mathrm{Im}(1/D)$ of Co(5 ML)/Ru(5 ML) is much smaller than that of HCP Co. The small value of $\mathrm{Im}(1/D)$ makes Kerr rotation angle (θ_K) small as seen in Eq. (1). In this way, we can understand that the large value of $\mathrm{Re}(\sigma_{xx})$ of HCP Ru has a significant role to decrease Kerr rotation angle of Co(5 ML)/Ru(5 ML) comparing with HCP Co.

The calculated off-diagonal conductivities ($\mathrm{Re}(\omega\sigma_{xy})$, $\mathrm{Im}(\omega\sigma_{xy})$) are shown in Fig. 4. We can see that $\mathrm{Im}(\omega\sigma_{xy})$ of Co(5ML)/Ru(5ML) is reduced to be about 1/3–1/4 of that of HCP Co. The lattice distortion of Co layers has a significant role in decreasing $\omega\sigma_{xy}$. In addition, the other effect considered to be mainly due to hybridization between Co and Ru layers also has a significant role since the $\omega\sigma_{xy}$ of Co(5 ML)/Ru(5 ML) is reduced to less than half of distorted HCP Co.

To observe the effect of hybridization between Co and Ru layers, we show the contribution to $\omega\sigma_{xy}$ from each Co layer compared to that of the distorted HCP Co in Fig. 5. From these figures, we can find that the

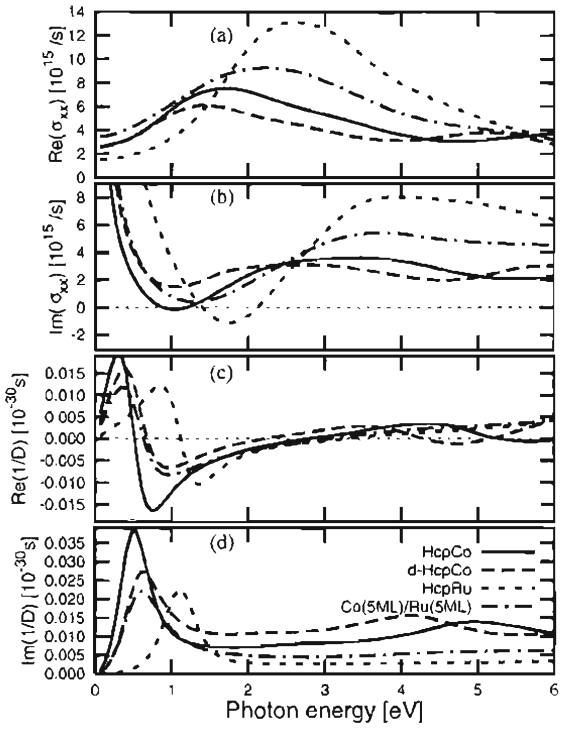

Fig. 3. Real and imaginary part of (a) and (b) the calculated diagonal optical conductivity ($\sigma_{xx}(\omega)$) and of (c) and (d) its contribution to Kerr and ellipticity spectra ($1/D$ in Eq. (1)). "d-Hcp Co" indicates the calculated result for distorted HCP Co.

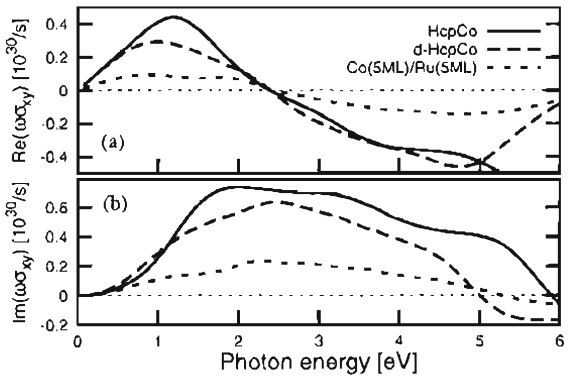

Fig. 4. (a) Real and (b) imaginary parts of the calculated off-diagonal optical conductivity $\omega\sigma_{xy}(\omega)$ of Co(5 ML)/Ru(5 ML), HCP CO, and distorted HCP Co.

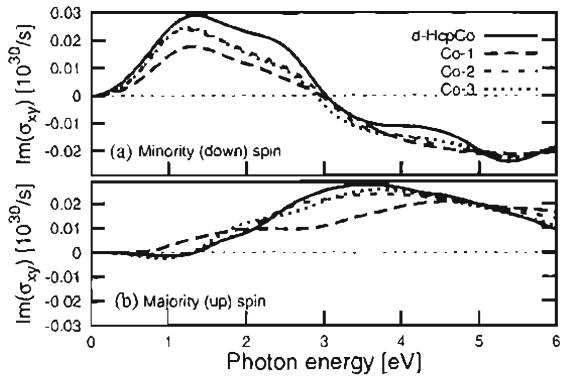

Fig. 5. Contributions to $\mathrm{Im}(\omega\sigma_{xy})$ from each spin ((a) minority, (b) majority) and each atom in Co(5ML)/Ru(5ML) and distorted HCP Co (d-HcpCo). "Co-1", "Co-2", and "Co-3" indicate the interfacial Co layer, the next Co layer, and central Co layer, respectively. For comparison, the result of d-HcpCo is scaled by the volume ratio between Co(5 ML)/Ru(5 ML) and d-HcpCo.

contribution from interfacial Co layer (Co-1) adjacent to a Ru layer is reduced by the hybridization effect. It should be noted that the effect of hybridization remains even in the central Co layer (Co-3).

The partial density of states (pDos) for Co(3d) and Ru(4d) of Co(5 ML)/Ru(5 ML) are shown in Fig. 6. For comparison, pDos of HCP Ru and distorted HCP Co are also shown. From these figures, we can find that the pDos of 3d state in interfacial Co layer (Co-1) is made to be wider in energy than the other Co layers. This makes pDos lower in density and also in spin–orbit splitting between $\pm m$ states, which causes the decrease of $\mathrm{Im}(\omega\sigma_{xy})$.

The estimated value of spin-orbit interaction of Ru 4d state is about 146 meV, which is about twice compared with that of Co 3d state (77 meV). However, the density of state for Ru 4d is wide in energy and low in density as seen in Fig. 6. This makes the spin–orbit splitting between $\pm m$ density of states smaller. In addition, the calculated magnetic moment of Ru is only up to about $0.05\,\mu_B$ in Co(5 ML)/Ru(5 ML). For these reasons, the spin–orbit interaction of Ru 4d state does not work effectively to enhance the magneto-optical effect in this superlattice.

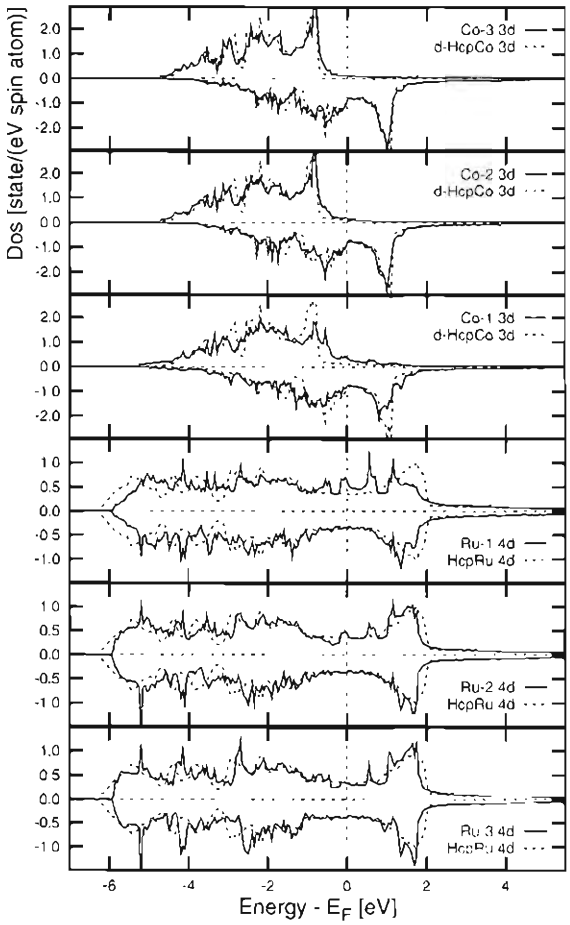

Fig. 6. The partial density of states for Co(3d) and Ru(4d) of Co(5ML)/Ru(5ML) comparing with those of HCP Ru and distorted HCP Co (d-Hcp Co). These figures are listed according to the order of stacking layers.

4. Summary

The magneto-optical Kerr effects in metallic superlattices fabricated by monatomic layer control were measured and compared with first-principles calculations. For Fe/Au, the measured Kerr for Fe(x ML)/Au(x ML) ($x = 1-6$) change systematically with increasing layer thickness x. For Co/Ru, the measured Kerr effect for ferromagnetic Co(5 ML)/Ru(5 ML) was very small compared to that of HCP Co. The calculated Kerr spectra from first-principles were in good agreement with experimental results. The Kerr rotation angle of Co(5 ML)/Ru(5 ML) is reduced by large σ_{xx} (diagonal optical conductivity) of HCP Ru, lattice distortion of Co layers, and strong hybridization between Ru 4d and Co 3d states.

Acknowledgements

This work was supported by Grant-in-Aids for Scientific Research from the Ministry of Education, Science, Sports and Culture, a JSPS Research Project for the Future Program (JSPS-RFTF 96P00106), and Special Coordination Funds for Promoting Science and Technology on "Nanohetero Metallic Materials" from the Science and Technology Agency. This work was performed under the interuniversity cooperative research program of IMR, Tohoku University, Tokyo University of Agriculture and Technology, and Japan Atomic Energy Research Institute. The authors thank Dr. S. Mitani, Tohoku University, for helpful discussions.

References

[1] K. Takanashi, S. Mitani, M. Sano, H. Fujimori, H. Nakajima, A. Osawa, Appl. Phys. Lett. 67 (1995) 1016.
[2] S. Mitani, K. Takanashi, H. Nakajima, K. Sato, R. Schreiber, P. Grunberg, H. Fujimori, J. Magn. Magn. Mater. 159 (1996) 7.
[3] K. Takanashi, S. Mitani, K. Himi, H. Fujimori, Appl. Phys. Lett. 72 (1998) 737.
[4] S.S.P. Parkin, N. More, K.P. Roche, Phys. Rev. Lett. 64 (1990) 2304.
[5] K. Ounadjela, D. Muller, A. Dinia, A. Arbaoui, P. Panissod, G. Suran, Phys. Rev. B 45 (1992) 7768.

[6] P.J.H. Bloemen, H.W. van Kesteren, H.J.M. Swagten, W.J.M. de Jonge, Phys. Rev. B 50 (1994) 13505.
[7] D. Muller, K. Ounadjela, P. Vennegues, V. Pierron-Bohnes, A. Arbaoui, J.P. Jay, A. Dinia, P. Panissod, J. Magn. Magn. Mater. 104–107 (1992) 1873.
[8] K. Himi, K. Takanashi, S. Mitani, M. Yamaguchi, D.H. Ping, K. Hono, H. Fujimori, Appl. Phys. Lett. 78 (2001) 1436.
[9] K. Takanashi, K. Himi, S. Mitani, M. Yamaguchi, D.H. Ping, K. Hono, H. Fujimori, Surf. Sci., in press.
[10] A. Yoshihara, Z.J. Wang, K. Takanashi, P. Grunberg, M. Motokawa, H. Fujimori, J. Magn. Soc. Jpn. 23 (1999) 161.
[11] A. Yoshihara, J.T. Wang, K Takanashi, K. Himi, Y. Kawazoe, H. Fujimori, P. Grünberg, Phys. Rev. B 63 (2001) 100405(R).
[12] K. Sato, E. Takeda, M. Akita, M. Yamaguchi, K. Takanashi, S. Mitani, H. Fujimori, Y. Suzuki, J. Appl. Phys. 86 (1999) 4985.
[13] M. Yamaguchi, T. Kusakabe, K. Kyuno, S. Asano, Physica B 270 (1999) 17.
[14] M. Yamaguchi, T. Kusakabe, K. Kyuno, S Asano, J. Magn. Soc. Jpn 22 (1998) 1401 (in Japanese).
[15] K. Sato, H. Hongu, H. Ikekame, Y. Tosaka, M. Watanabe, K. Takanashi, H. Fujimori, Jpn. J. Appl. Phys. 32 Part 1 (1993) 989.
[16] C.S. Wang, J. Callaway, Phys. Rev. B 9 (1974) 4897.
[17] D. Weller, G.R. Harp, R.F.C. Farrow, A. Cebollada, J. Sticht, Phys. Rev. Lett. 72 (1994) 2097.